

IEEE Copyright Notice

- ©20xx IEEE. Personal use of this material is permitted. However, permission to reprint/republish this material for advertising or promotional purposes or for creating new collective works for resale or redistribution to servers or lists, or to reuse any copyrighted component of this work in other works must be obtained from the IEEE.
- This material is presented to ensure timely dissemination of scholarly and technical work. Copyright and all rights therein are retained by authors or by other copyright holders. All persons copying this information are expected to adhere to the terms and constraints invoked by each author's copyright. In most cases, these works may not be reposted without the explicit permission of the copyright holder.

Generalized Adaptive Notch Smoothers for Real-Valued Signals and Systems

Maciej Niedźwiecki and Adam Sobociński

Abstract—Systems with quasi-periodically varying coefficients can be tracked using the algorithms known as generalized adaptive notch filters (GANFs). GANF algorithms can be considered an extension, to the system case, of classical adaptive notch filters (ANFs). We show that estimation accuracy of the existing algorithms, as well as their robustness to the choice of design parameters, can be considerably improved by means of compensating estimation delay effects which occur in the amplitude tracking and frequency tracking loops of GANF/ANF filters. Apart from the increased computational burden, the price for the achieved improvements is paid in terms of a decision delay—the proposed generalized adaptive notch smoothing (GANS) algorithms must be run on delayed input/output data sequences. Since such delay is acceptable in many signal processing and system identification applications, the proposed solution seems to be an attractive alternative to the currently available trackers.

Index Terms—Adaptive notch filters (ANF), frequency estimation, identification of nonstationary systems.

I. INTRODUCTION

GENERALIZED ADAPTIVE NOTCH FILTERS (GANFs) [1] are system identification algorithms used to track parameters of quasi-periodically varying processes, i.e., processes governed by

$$\begin{aligned}
 y(t) &= \sum_{l=1}^n \theta_l(t) \varphi_l(t) + v(t) = \boldsymbol{\varphi}^T(t) \boldsymbol{\theta}(t) + v(t) \\
 \theta_l(t) &= a_{l,0}(t) + \sum_{i=1}^k b_{l,i}(t) \sin(\phi_i(t) + \phi_{l,i}^0) \\
 &= a_{l,0}(t) + \sum_{i=1}^k [a_{l,2i-1}(t) \sin \phi_i(t) \\
 &\quad + a_{l,2i}(t) \cos \phi_i(t)] \\
 \phi_i(t) &= \sum_{s=1}^t \omega_i(s) \\
 a_{l,2i-1}(t) &= b_{l,i}(t) \cos(\phi_{l,i}^0) \\
 a_{l,2i}(t) &= b_{l,i}(t) \sin(\phi_{l,i}^0) \\
 l &= 1, \dots, n
 \end{aligned} \tag{1}$$

Manuscript received November 11, 2006; revised May 19, 2007. The associate editor coordinating the review of this manuscript and approving it for publication was Dr. Vitor Heloiz Nascimento. This work was supported by MNiSW by Grant N514 011 31/3091.

The authors are with the Faculty of Electronics, Telecommunications and Computer Science, Department of Automatic Control, Gdańsk University of Technology, Gdańsk, Poland (e-mail: maciekn@eti.pg.gda.pl; adsob@eti.pg.gda.pl).

Digital Object Identifier 10.1109/TSP.2007.906747

where $y(t)$ denotes the system output, $\boldsymbol{\varphi}(t) = [\varphi_1(t), \dots, \varphi_n(t)]^T$ is the regression vector made up of the measurable input signals, $\boldsymbol{\theta}(t) = [\theta_1(t), \dots, \theta_n(t)]^T$ is the vector of time varying coefficients, and $v(t)$ denotes zero-mean white measurement noise.

Each system coefficient is modeled as a linear combination of k sinusoidal signals with slowly varying amplitudes $b_{l,i}(t)$ and slowly varying frequencies $\omega_i(t) \in [-\pi, \pi]$. We note that some rapidly fading telecommunication channels admit such parametrization [2]–[5].

Consider a system with a single ($k = 1$) nonzero frequency mode (we will extend our analysis to the multiple-frequency case later)

$$\theta_l(t) = a_{l,1}(t) \sin \phi(t) + a_{l,2}(t) \cos \phi(t), \quad l = 1, \dots, n$$

$$\phi(t) = \sum_{s=1}^t \omega(s)$$

and let

$$\begin{aligned}
 \boldsymbol{\alpha}(t) &= [a_{1,1}(t), a_{1,2}(t), \dots, a_{n,1}(t), a_{n,2}(t)]^T \\
 \mathbf{f}(t) &= [\sin \phi(t), \cos \phi(t)]^T \\
 \mathbf{h}(t) &= [\cos \phi(t), -\sin \phi(t)]^T \\
 \boldsymbol{\psi}(t) &= \boldsymbol{\varphi}(t) \otimes \mathbf{f}(t) \\
 \boldsymbol{\chi}(t) &= \boldsymbol{\varphi}(t) \otimes \mathbf{h}(t) \\
 \mathbf{G}(t) &= \begin{bmatrix} \cos \omega(t) & \sin \omega(t) \\ -\sin \omega(t) & \cos \omega(t) \end{bmatrix}
 \end{aligned}$$

where \otimes denotes the Kronecker product of the respective matrices/vectors.

Note that in the case considered above, (1) can be rewritten in an equivalent form as

$$y(t) = \boldsymbol{\psi}^T(t) \boldsymbol{\alpha}(t) + v(t). \tag{2}$$

For a single-mode system subject to a wide-sense stationary excitation $\{\boldsymbol{\varphi}(t)\}$ with known covariance matrix $\boldsymbol{\Phi} = E[\boldsymbol{\varphi}(t) \boldsymbol{\varphi}^T(t)] > 0$, the normalized steady state version of the GANF algorithm presented in [1] can be written down in the form

$$\begin{aligned}
 \hat{\mathbf{f}}(t) &= \hat{\mathbf{G}}(t) \hat{\mathbf{f}}(t-1) \\
 \hat{\mathbf{h}}(t) &= \hat{\mathbf{G}}(t) \hat{\mathbf{h}}(t-1) = \mathbf{J} \hat{\mathbf{f}}(t) \\
 \hat{\boldsymbol{\psi}}(t) &= \boldsymbol{\varphi}(t) \otimes \hat{\mathbf{f}}(t) \\
 \hat{\boldsymbol{\chi}}(t) &= \boldsymbol{\varphi}(t) \otimes \hat{\mathbf{h}}(t)
 \end{aligned}$$

$$\begin{aligned}
\varepsilon(t) &= y(t) - \hat{\boldsymbol{\psi}}^T(t)\hat{\boldsymbol{\alpha}}(t-1) \\
\hat{\boldsymbol{\alpha}}(t) &= \hat{\boldsymbol{\alpha}}(t-1) + \mu(\boldsymbol{\Phi}^{-1} \otimes \mathbf{I}_2)\hat{\boldsymbol{\psi}}(t)\varepsilon(t) \\
g(t) &= \frac{\hat{\boldsymbol{\chi}}^T(t)\hat{\boldsymbol{\alpha}}(t-1)\varepsilon(t)}{\hat{\boldsymbol{\alpha}}^T(t)(\boldsymbol{\Phi} \otimes \mathbf{I}_2)\hat{\boldsymbol{\alpha}}(t)} \\
\hat{\omega}(t+1) &= \hat{\omega}(t) + \gamma g(t) \\
\hat{\boldsymbol{\theta}}(t) &= (\mathbf{I}_n \otimes \hat{\mathbf{f}}^T(t))\hat{\boldsymbol{\alpha}}(t)
\end{aligned} \tag{3}$$

where \mathbf{I}_n denotes the $n \times n$ identity matrix

$$\hat{\mathbf{G}}(t) = \begin{bmatrix} \cos \hat{\omega}(t) & \sin \hat{\omega}(t) \\ -\sin \hat{\omega}(t) & \cos \hat{\omega}(t) \end{bmatrix}, \quad \mathbf{J} = \begin{bmatrix} 0 & 1 \\ -1 & 0 \end{bmatrix}$$

and the initial conditions are set to $\hat{\mathbf{f}}(0) = \mathbf{f}_o = [0, 1]^T$ and $\hat{\mathbf{h}}(0) = \mathbf{h}_o = [1, 0]^T$.

Tracking properties of this algorithm are determined by two user-dependent tuning coefficients: the adaptation gain $\mu, 0 < \mu \ll 1$, which controls the rate of amplitude adaptation, and another adaptation gain $\gamma, 0 < \gamma \ll \mu$, which decides upon the rate of frequency adaptation. It is worth noticing that when the frequency $\omega(t)$ drifts according to the random walk model—which is one of the testbeds for comparing efficacy of different solutions—the optimally tuned complex-valued counterpart of (3) is, under Gaussian assumptions, a statistically efficient estimation procedure, i.e., it attains the posterior Cramér-Rao bound which limits performance of any tracking scheme [6].

In the special case where $n = 1$ and $\varphi(t) \equiv 1$, the model (1) becomes a description of a noisy nonstationary multifrequency signal. Under such circumstances GANF algorithm turns into an “ordinary” adaptive notch filter (ANF)—device used to either extract or suppress nonstationary sinusoidal signals buried in noise. Adaptive notch filters are used for a variety of purposes such as line enhancement [7], mitigation of narrowband interferences in communication channels [8], active noise and vibration control [9], [10] and biomedical signal processing [11]–[13], among many others.

Note that in the single frequency case ($k = 1$) where

$$y(t) = s(t) + v(t), \quad s(t) = a_1(t) \sin \phi(t) + a_2(t) \cos \phi(t)$$

and $\boldsymbol{\alpha}(t) = [a_1(t), a_2(t)]^T$, the signal-oriented version of (3) can be written down in the form

$$\begin{aligned}
\hat{\mathbf{f}}(t) &= \hat{\mathbf{G}}(t)\hat{\mathbf{f}}(t-1) \\
\hat{\mathbf{h}}(t) &= \mathbf{J}\hat{\mathbf{f}}(t) \\
\varepsilon(t) &= y(t) - \hat{\mathbf{f}}^T(t)\hat{\boldsymbol{\alpha}}(t-1) \\
\hat{\boldsymbol{\alpha}}(t) &= \hat{\boldsymbol{\alpha}}(t-1) + \mu\hat{\mathbf{f}}(t)\varepsilon(t) \\
g(t) &= \frac{\hat{\mathbf{h}}^T(t)\hat{\boldsymbol{\alpha}}(t-1)\varepsilon(t)}{\hat{\boldsymbol{\alpha}}^T(t)\hat{\boldsymbol{\alpha}}(t)} \\
\hat{\omega}(t+1) &= \hat{\omega}(t) + \gamma g(t) \\
\hat{s}(t) &= \hat{\mathbf{f}}^T(t)\hat{\boldsymbol{\alpha}}(t).
\end{aligned} \tag{4}$$

As shown in [1], tuning of the GANF/ANF algorithms (3) and (4) requires compromising two contradictory requirements. On

one hand, one should maintain satisfactory noise rejection capability of the filter, which decreases with growing gains μ and γ . On the other hand, one should maximize the filter’s tracking speed, which increases with growing adaptation gains. From the statistical viewpoint this is a tradeoff between the variance and bias components of the mean-squared tracking error. The variance component is caused by fluctuations of parameter estimates around their mean values. The bias component of the tracking error originates from the fact that mean trajectories of parameter estimates lag behind the true parameter trajectories (for this reason bias errors are often called lag errors). In our current context it means, roughly speaking, that $\hat{\boldsymbol{\alpha}}(t)$ and $\hat{\omega}(t)$ can be viewed as the estimates of $\boldsymbol{\alpha}(t-t_\alpha)$ and $\omega(t-t_\omega)$, respectively—rather than of $\boldsymbol{\alpha}(t)$ and $\omega(t)$ —where t_α and t_ω denote the corresponding estimation delays. We will show that estimation accuracy of GANF/ANF algorithms, as well as their robustness to the choice of design parameters, can be considerably increased by compensating both delays. This can be achieved by incorporating into the adaptive loop a decision delay of $t_o = t_\omega + t_\alpha$ sampling intervals. Even though impractical in adaptive prediction/control applications—to predict or control system’s behavior one needs to know a good model of its current dynamics and *not* of its past dynamics—such delay is acceptable in many signal processing (e.g., line enhancement) and system identification (e.g., channel equalization) applications. The estimation delay problem was studied in our earlier paper [14]. The contribution of the current paper is twofold. First, we extend results derived in [14] for a complex-valued GANF algorithm, to its real-valued counterpart. Second, and more importantly, in addition to the frequency delay compensation suggested earlier, we propose a new amplitude delay compensation mechanism. The resulting three-step algorithm performs better than the two-step algorithm described in [14].

The paper is organized as follows. The estimation delay effects occurring in the frequency tracking loop of the real-valued GANF algorithm are studied in Section II. Based on the analytical results, the two-step generalized notch smoother is proposed. Section III is devoted to analysis of the amplitude tracking loop of GANF. After deriving expression for the amplitude delay, the three-step estimation procedure, which combines the debiased amplitude and phase (frequency) information is designed. The multiple-frequency version of the generalized adaptive notch smoother is presented in Section IV. Section V shows the results of simulation experiments. Finally, Section VI concludes.

II. FREQUENCY TRACKING LOOP

A. Analysis

Frequency estimates yielded by the GANF algorithm are biased. Suppose that $\boldsymbol{\alpha}(t) = \boldsymbol{\alpha}_o, \forall t$, which means that the changes of $\boldsymbol{\theta}(t)$ can be attributed exclusively to the changes in $\omega(t)$. Then, using the approximating linear filter technique and the deterministic averaging approach, one can show that (see Appendix)

$$\hat{\omega}(t) \cong (1 - q^{-1})F(q^{-1})\nu(t) + F(q^{-1})\omega(t), \tag{5}$$

where q^{-1} denotes the backward shift operator

$$\begin{aligned} \nu(t) &= 2\alpha_o \chi(t) v(t) / b^2 \\ b^2 &= \alpha_o^T (\Phi \otimes \mathbf{I}_2) \alpha_o \\ F(q^{-1}) &= \frac{(1 - \delta)q^{-1}}{1 - (\lambda + \delta)q^{-1} + \lambda q^{-2}} \end{aligned}$$

and $\lambda = 1 - \mu/2$, $\delta = 1 - \gamma/2$. The filter $F(q^{-1})$ is asymptotically stable for all values of $\lambda, \delta \in (0, 1)$.

Denote by $\omega_{av}(t) = E[\hat{\omega}(t)|\omega(s), s \leq t]$ the mean path of frequency estimates. Assuming that $\{v(t)\}$ is a zero-mean white noise, independent of $\{\varphi(t)\}$ and $\{\omega(t)\}$, one obtains $E[\nu(t)|\omega(s), s \leq t] = E[\nu(t)] = 0$, which leads to the following relationship between the mean values of frequency estimates $\omega_{av}(t)$ and true frequency values $\omega(t)$

$$\omega_{av}(t) \cong F(q^{-1})\omega(t). \quad (6)$$

Since the filter $F(q^{-1})$ is lowpass, for a slowly varying frequency the signal, $\{\omega_{av}(t)\}$ can be regarded a time-shifted version of $\{\omega(t)\}$. A good measure of this shift can be obtained by evaluating the nominal (low-frequency) phase or group delay of the filter $F(e^{-j\xi}) = A_F(\xi)e^{j\phi_F(\xi)}$ (ξ denotes the standard Fourier-domain frequency variable)

$$\tau_\omega = -\lim_{\xi \rightarrow 0} \frac{\phi_F(\xi)}{\xi} = -\lim_{\xi \rightarrow 0} \frac{d\phi_F(\xi)}{d\xi} = \frac{\mu}{\gamma}. \quad (7)$$

This means that the (approximately) debiased estimate of the instantaneous frequency $\omega(t)$ can be obtained from

$$\bar{\omega}(t) = \hat{\omega}(t + t_\omega) \quad (8)$$

where $t_\omega = \text{int}[\tau_\omega]$ and $\text{int}[x]$ denotes an integer number that is closest to x .

Remark: The problem of determining the estimation bandwidth of generalized adaptive notch filters, i.e., the range in which frequency changes can be tracked “successfully,” was considered in [6] and [19] for a system with frequency changes governed by the random walk model: $\omega(t) = \omega(t-1) + w(t)$ where $\{w(t)\}$, $\text{var}[w(t)] = \sigma_w^2$, denotes the white noise sequence, independent of $\{v(t)\}$ and $\{\varphi(t)\}$. For the complex-valued GANF, operating under Gaussian assumptions, good tracking is guaranteed when

$$\sigma_w \leq \frac{0.01}{\sqrt{2n \text{ SNR}}}$$

where $\text{SNR} = (\sigma_y^2 - \sigma_v^2) / \sigma_v^2$ denotes the signal-to-noise ratio (SNR). Even though the analogous results for the real-valued GANF were not established yet, the above condition is certainly a good guideline also in the real case.

One should not be surprised by the fact that the right-hand side of the inequality given above depends on the number of estimated coefficients n —as argued in [17, Ch. 2], the larger the number of unknown coefficients, the more difficult the corresponding tracking problem.

B. Two-Step Generalized Adaptive Notch Smoothing (GANS) Algorithm

The debiased frequency estimates $\bar{\omega}(t)$ can be used to compute more accurate estimates of systems parameters. A simple way of doing this, which was suggested in [14] for complex-valued GANF algorithms, is run—in addition to (3)—the following “frequency-guided” GANF algorithm

$$\begin{aligned} \tilde{\varepsilon}(t) &= y(t) - \bar{\boldsymbol{\psi}}^T(t) \tilde{\boldsymbol{\alpha}}(t-1) \\ \tilde{\boldsymbol{\alpha}}(t) &= \tilde{\boldsymbol{\alpha}}(t-1) + \mu(\Phi^{-1} \otimes \mathbf{I}_2) \bar{\boldsymbol{\psi}}(t) \tilde{\varepsilon}(t) \\ \tilde{\boldsymbol{\theta}}(t) &= (\mathbf{I}_n \otimes \bar{\mathbf{f}}^T(t)) \tilde{\boldsymbol{\alpha}}(t) \end{aligned} \quad (9)$$

where

$$\bar{\boldsymbol{\psi}}(t) = \boldsymbol{\varphi}(t) \otimes \bar{\mathbf{f}}(t), \quad \bar{\mathbf{f}}(t) = [\sin \bar{\phi}(t), \cos \bar{\phi}(t)]^T$$

and

$$\bar{\phi}(t) = \sum_{s=1}^t \bar{\omega}(s) = \sum_{s=1}^t \hat{\omega}(s + t_\omega)$$

denotes the debiased phase.

The function $\bar{\mathbf{f}}(t)$ can be computed recursively using

$$\begin{aligned} \bar{\mathbf{f}}(t) &= \bar{\mathbf{G}}(t) \bar{\mathbf{f}}(t-1), \quad t > 0, \quad \bar{\mathbf{f}}(0) = \mathbf{f}_o \\ \bar{\mathbf{G}}(t) &= \begin{bmatrix} \cos \bar{\omega}(t) & \sin \bar{\omega}(t) \\ -\sin \bar{\omega}(t) & \cos \bar{\omega}(t) \end{bmatrix}. \end{aligned}$$

Since at each time instant the algorithm (9) incorporates frequency estimates $\bar{\omega}(t) = \hat{\omega}(t + t_\omega)$ yielded by the “pilot” algorithm (3), which depend on all past data samples and on t_ω “future” data samples, the two-step procedure (3) and (9) is a fixed-lag smoother. It will be further referred to as a two-step GANS. As all noncausal filters, GANS must be run on delayed input/output data sequences. We note that the resulting decision delay of t_ω sampling intervals, which must be incorporated into the adaptive loop, is acceptable in many signal processing and system identification applications.

III. AMPLITUDE TRACKING LOOP

A. Analysis

To reveal the delay structure embedded in estimation of $\boldsymbol{\alpha}(t)$ we will assume, for the time being, that the time-varying instantaneous frequencies $\omega(t)$ are known exactly. Even though obviously violated by the original GANF algorithm (3), this assumption is approximately fulfilled (for small values of μ and sufficiently slow frequency variations) by the frequency-guided filter (9).

Setting $\bar{\omega}(t) \equiv \omega(t)$ in (9), which entails $\bar{\boldsymbol{\psi}}(t) \equiv \boldsymbol{\psi}(t)$ and $\bar{\mathbf{f}}(t) \equiv \mathbf{f}(t)$, one arrives at

$$\begin{aligned} \tilde{\varepsilon}(t) &= y(t) - \boldsymbol{\psi}^T(t) \tilde{\boldsymbol{\alpha}}(t-1) \\ \tilde{\boldsymbol{\alpha}}(t) &= \tilde{\boldsymbol{\alpha}}(t-1) + \mu(\Phi^{-1} \otimes \mathbf{I}_2) \boldsymbol{\psi}(t) \tilde{\varepsilon}(t) \\ \tilde{\boldsymbol{\theta}}(t) &= (\mathbf{I}_n \otimes \mathbf{f}^T(t)) \tilde{\boldsymbol{\alpha}}(t). \end{aligned} \quad (10)$$

Denote by $\Delta \tilde{\boldsymbol{\alpha}}(t) = \tilde{\boldsymbol{\alpha}}(t) - \boldsymbol{\alpha}(t)$ the estimation error and by $\Delta \boldsymbol{\alpha}(t) = \boldsymbol{\alpha}(t) - \boldsymbol{\alpha}(t-1)$ —the one-step change in $\boldsymbol{\alpha}(t)$.

Combining (2) with (10) one obtains, after straightforward calculations

$$\begin{aligned} \Delta\tilde{\alpha}(t) &= (\mathbf{I}_{2n} - \mu(\Phi^{-1} \otimes \mathbf{I}_2)\psi(t)\psi^T(t))\Delta\tilde{\alpha}(t-1) \\ &\quad - (\mathbf{I}_{2n} - \mu(\Phi^{-1} \otimes \mathbf{I}_2)\psi(t)\psi^T(t))\Delta\alpha(t) \\ &\quad + \mu(\Phi^{-1} \otimes \mathbf{I}_2)\psi(t)v(t). \end{aligned} \quad (11)$$

We have assumed that $\alpha(t)$ is a slowly varying quantity. Since, for small adaptation gains, the estimate $\hat{\alpha}(t)$ also varies slowly compared to $\varphi(t)$ and $f(t)$, we can analyze (11) using the deterministic averaging approach.

Denote by

$$\langle x(t) \rangle_T = \frac{1}{T} \sum_{i=0}^{T-1} x(t-i)$$

the local average of $x(t)$, and by

$$\langle x(t) \rangle_\infty = \lim_{T \rightarrow \infty} \langle x(t) \rangle_T$$

the corresponding limiting value (assuming it exists).

For sufficiently slow frequency variations $\sin \phi(t)$ and $\cos \phi(t)$ are locally almost periodic functions of time: $\sin \phi(t-i) \cong \sin(\omega_o(t-i))$, $\cos \phi(t-i) \cong \cos(\omega_o(t-i))$, $i \in [0, T-1]$, where $\omega_o = \dot{\phi}(t)/t$. As argued in [1], when $T \gg 2\pi/\omega_o$ and when the process $\{\varphi(t)\}$ is nondeterministic second-order stationary and ergodic it holds that

$$\begin{aligned} \langle \psi(t)\psi^T(t) \rangle_T &= \langle (\varphi(t)\varphi^T(t)) \otimes (f(t)f^T(t)) \rangle_T \\ &\cong \langle \psi(t)\psi^T(t) | \omega(t) \equiv \omega_o \rangle_\infty = \frac{1}{2} \Phi \otimes \mathbf{I}_2. \end{aligned}$$

Applying local averaging to (11), and noting that $(\Phi^{-1} \otimes \mathbf{I}_2)(\Phi \otimes \mathbf{I}_2) = \mathbf{I}_n \otimes \mathbf{I}_2 = \mathbf{I}_{2n}$ one arrives at

$$\Delta\tilde{\alpha}(t) \cong \lambda\Delta\tilde{\alpha}(t-1) - \lambda\Delta\alpha(t) + \mu(\Phi^{-1} \otimes \mathbf{I}_2)\psi(t)v(t)$$

or equivalently

$$\tilde{\alpha}(t) \cong G(q^{-1})\zeta(t) + G(q^{-1})\alpha(t) \quad (12)$$

where

$$\begin{aligned} \zeta(t) &= 2(\Phi^{-1} \otimes \mathbf{I}_2)\psi(t)v(t) \\ G(q^{-1}) &= \frac{\mu}{2(1 - \lambda q^{-1})}. \end{aligned}$$

Denote by $\alpha_{av}(t) = E[\tilde{\alpha}(t)|\alpha(s), s \leq t]$ the mean path of the amplitude estimates. After taking expectations of both sides of (12) one arrives at

$$\alpha_{av}(t) = G(q^{-1})\alpha(t).$$

Since the nominal delay of the filter $G(e^{-j\xi}) = A_G(\xi)e^{j\phi_G(\xi)}$ is equal to

$$\tau_\alpha = -\lim_{\xi \rightarrow 0} \frac{\phi_G(\xi)}{\xi} = -\lim_{\xi \rightarrow 0} \frac{d\phi_G(\xi)}{d\xi} = \frac{2\lambda}{\mu} \quad (13)$$

the approximately debiased estimate of $\alpha(t)$ can be obtained from

$$\bar{\alpha}(t) = \tilde{\alpha}(t + t_\alpha) \quad (14)$$

where $t_\alpha = \text{int}[\tau_\alpha]$.

Remark: Estimation delays arising in the frequency tracking loops of the real-valued GANF (3) and its complex-valued coun-

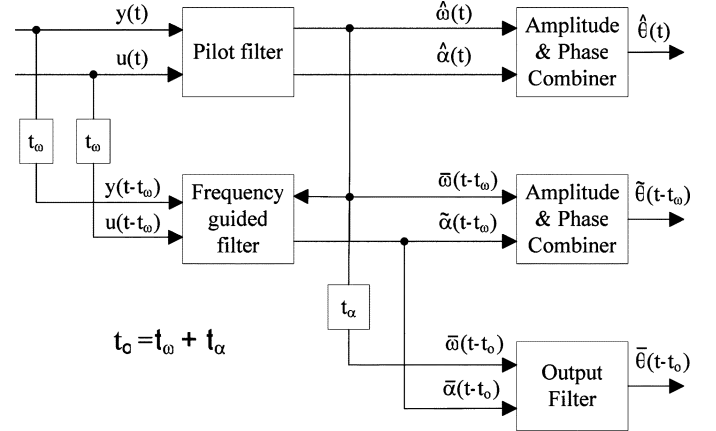


Fig. 1. Block diagram of a three-step GANS.

terpart, described in [14], are identical. In the case of amplitude tracking, the situation is different. When the amplitude tracking loop of the complex-valued algorithm is analyzed, one arrives at $\tau_\alpha = \lambda/\mu$, which means that the associated delay is approximately two times smaller than the one established above. This shows that the results derived for the complex-valued case cannot be mechanically extended to the real-valued case, and vice versa.

B. Three-Step GANS Algorithm

The debiased three-step estimate of $\theta(t)$ can be obtained by combining the debiased phase and amplitude components, namely

$$\begin{aligned} \bar{\theta}(t) &= (\mathbf{I}_n \otimes \bar{\mathbf{f}}^T(t))\bar{\alpha}(t) \\ &= (\mathbf{I}_n \otimes \hat{\mathbf{f}}^T(t + t_\omega))\tilde{\alpha}(t + t_\alpha). \end{aligned} \quad (15)$$

The associated decision delay is equal to $t_o = t_\omega + t_\alpha$ sampling intervals. The block diagram of the three-step GANS is shown in Fig. 1.

Denote by $s(t) = \varphi^T(t)\theta(t)$ the noiseless system output. The following symbols will be further used:

$$\hat{s}(t) = \varphi^T(t)\hat{\theta}(t), \quad \tilde{s}(t) = \varphi^T(t)\tilde{\theta}(t), \quad \bar{s}(t) = \varphi^T(t)\bar{\theta}(t)$$

to denote the estimates of $s(t)$ associated with the GANF estimate $\hat{\theta}(t)$, the two-step GANS estimate $\tilde{\theta}(t)$ and the three-step GANS estimate $\bar{\theta}(t)$, respectively.

The idea of “smoothing by means of delayed filtering” is not new. In the classical papers of Hedelin [15] and Hedelin and Jönson [16] it was shown that the appropriately delayed state estimates yielded by the Kalman filter are close, in the mean square sense, to those provided by the Kalman smoother. Even though our concept is similar to that described in [15] and [16], there are some important qualitative differences. In the case of Kalman filtering/smoothing there seems to be no way to analytically determine the optimal delay; the situation is further complicated by the fact that, in principle, different lags should be considered for different components of the state vector. This means that all one can do in practice is find out the lags experimentally for a given (time-invariant) system at hand. In contrast with this, the estimation delays t_α and t_ω , which occur

in the amplitude tracking and frequency tracking loops of the GANF algorithm, do not depend on parameters of the identified quasi-periodically varying system; both delays are known functions of adaptation gains and, as such, they can be easily precomputed and compensated.

IV. MEAN-SQUARE ERROR ANALYSIS

Denote by $\Delta\hat{\omega}(t, \tau) = \hat{\omega}(t) - \omega(t - \tau)$ and $\Delta\tilde{\alpha}(t, \tau) = \tilde{\alpha}(t) - \alpha(t - \tau)$ the frequency and amplitude matching errors, respectively. The term ‘‘matching errors’’ was introduced in [17] to characterize performance of adaptive systems which incorporate a decision delay of τ sampling intervals. When τ is equal to zero, matching errors are identical with tracking errors. According to (5) and (12) it holds that

$$\begin{aligned}\Delta\hat{\omega}(t, \tau) &\cong (1 - q^{-1})F(q^{-1})\nu(t) + [F(q^{-1}) - q^{-\tau}]\omega(t) \\ \Delta\tilde{\alpha}(t, \tau) &\cong G(q^{-1})\zeta(t) + [G(q^{-1}) - q^{-\tau}]\alpha(t).\end{aligned}$$

To gain insight into the parameter matching behavior of GANS we will assume that the sequences $\{\omega(t)\}$ and $\{\alpha(t)\}$ are zero-mean wide-sense stationary processes with spectral density functions $S_\omega(\xi)$ and $S_\alpha(\xi)$, respectively.

Using standard results from the linear filtering theory [18] one obtains

$$\begin{aligned}\langle E[(\Delta\hat{\omega}(t, \tau))^2] \rangle_T &\cong \frac{\langle \sigma_\nu^2(t) \rangle_T}{2\pi} \int_{-\pi}^{\pi} V_\omega(\xi) d\xi \\ &+ \frac{1}{2\pi} \int_{-\pi}^{\pi} B_\omega(\xi, \tau) S_\omega(\xi) d\xi\end{aligned}\quad (16)$$

where

$$\begin{aligned}V_\omega(\xi) &= |(1 - e^{-j\xi})F(e^{-j\xi})|^2 \\ B_\omega(\xi, \tau) &= |F(e^{-j\xi}) - e^{-j\xi\tau}|^2\end{aligned}$$

and the expectation is taken over different realizations of the measurement noise and different realizations of frequency trajectory. One can show that [1] $\langle \chi(t)\chi^T(t) \rangle_T \cong (1/2)(\Phi \otimes \mathbf{I}_2)$ and therefore $\langle \sigma_\nu^2(t) \rangle_T \cong 2\sigma_v^2/b^2$.

The first term on the right-hand side (RHS) of (16) describes the variance component of the mean-square frequency matching error, and the second term constitutes its bias component.

In a similar way one can analyze the mean-square amplitude matching errors, arriving at

$$\begin{aligned}\langle E[\|\Delta\tilde{\alpha}(t, \tau)\|^2] \rangle_T &\cong \frac{\text{tr}\{\langle \text{cov}[\zeta(t)] \rangle_T\}}{2\pi} \int_{-\pi}^{\pi} V_\alpha(\xi) d\xi \\ &+ \frac{1}{2\pi} \int_{-\pi}^{\pi} B_\alpha(\xi, \tau) \text{tr}\{S_\alpha(\xi)\} d\xi\end{aligned}\quad (17)$$

where

$$\begin{aligned}V_\alpha(\xi) &= |G(e^{-j\xi})|^2 \\ B_\alpha(\xi, \tau) &= |G(e^{-j\xi}) - e^{-j\xi\tau}|^2.\end{aligned}$$

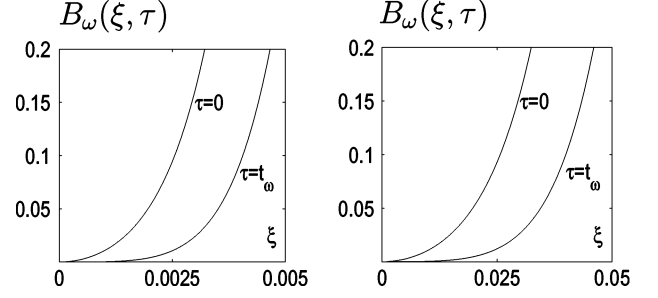


Fig. 2. Frequency bias characteristics $B_\omega(\xi, \tau)$ for the original GANF algorithm ($\tau = 0$) and its bias-compensated version ($\tau = t_\omega$) for two different values of μ ($\gamma = \mu^2$): $\mu = 0.01$ (left figure) and $\mu = 0.1$ (right figure). Note the horizontal scale difference between the left figure and the right figure.

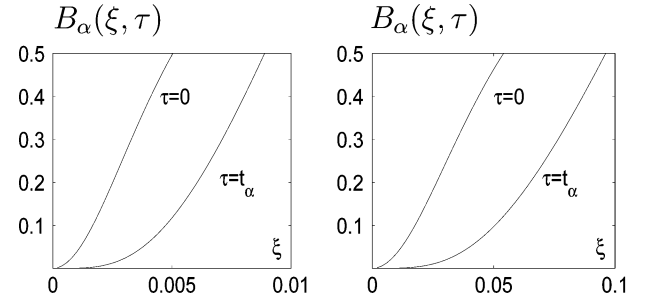


Fig. 3. Amplitude bias characteristics $B_\alpha(\xi, \tau)$ for the original GANF algorithm ($\tau = 0$) and its bias-compensated version ($\tau = t_\alpha$) for two different values of μ ($\gamma = \mu^2$): $\mu = 0.01$ (left figure) and $\mu = 0.1$ (right figure). Note the horizontal scale difference between the left figure and the right figure.

Note that $\langle \text{cov}[\zeta(t)] \rangle_T = 4\sigma_v^2(\Phi^{-1} \otimes \mathbf{I}_2) \langle \psi(t)\psi^T(t) \rangle_T (\Phi^{-1} \otimes \mathbf{I}_2) \cong 2\sigma_v^2(\Phi^{-1} \otimes \mathbf{I}_2)$ and, hence, using the identity $\text{tr}\{\mathbf{A} \otimes \mathbf{B}\} = \text{tr}\{\mathbf{A}\}\text{tr}\{\mathbf{B}\}$ which holds for any square matrices \mathbf{A} and \mathbf{B} , one obtains $\text{tr}\{\langle \text{cov}[\zeta(t)] \rangle_T\} \cong \sigma_v^2 \text{tr}\{\Phi^{-1}\}$.

Since the variance components of the analyzed mean-square matching errors do not depend on the delay τ , to examine the influence of τ on performance of GANS it is sufficient to focus on the bias error components.

Fig. 2 shows the plots of the bias characteristics $B_\omega(\xi, 0)$ and $B_\omega(\xi, t_\omega)$ for two values of μ : $\mu = 0.01$ and $\mu = 0.1$. To reduce the number of design degrees of freedom, the gain γ was set to μ^2 (see comment in Section V). Fig. 3 shows the analogous plots of $B_\alpha(\xi, 0)$ and $B_\alpha(\xi, t_\alpha)$.

Note that compensation of the estimation delays allows one to considerably widen the stopband regions of both bias characteristics. Therefore, for slow frequency and amplitude variations (which guarantees that the dominant parts of the spectral density functions $S_\omega(\xi)$ and $S_\alpha(\xi)$ fall into the stopband regions of $B_\omega(\xi, \tau)$ and $B_\alpha(\xi, \tau)$), the bias components of the estimation errors will be smaller for GANS than for GANF. Since the variance components are for both algorithms identical, GANS should work *uniformly* better than GANF, i.e., it should yield better results for *all* values of adaptation gains and for *all* values of the SNR. Experimental results, presented in Section VI, fully confirm this claim.

Remark: The delay compensation technique is universal, i.e., it is not restricted to the algorithms described above. In principle, performance of *any* existing GANF/ANF algorithm can be improved in this way. Of course, in order to use this approach

one should be able to either compute or estimate delays arising in the corrected algorithm, which in many cases may be a non-trivial task.

V. MULTIPLE FREQUENCIES CASE

Using the technique described in [19, Section III.C], the multiple-frequency GANS procedure can be obtained by combining k single-frequency algorithms, described above, into a parallel structure of the following form.

Pilot Filter:

$$\begin{aligned}
\hat{\mathbf{f}}_i(t) &= \hat{\mathbf{G}}_i(t)\hat{\mathbf{f}}_i(t-1) \\
\hat{\mathbf{h}}_i(t) &= \mathbf{J}\hat{\mathbf{f}}_i(t) \\
\hat{\boldsymbol{\psi}}_i(t) &= \boldsymbol{\varphi}(t) \otimes \hat{\mathbf{f}}_i(t) \\
\hat{\boldsymbol{\chi}}_i(t) &= \boldsymbol{\varphi}(t) \otimes \hat{\mathbf{h}}_i(t) \\
i &= 1, \dots, k \\
\varepsilon(t) &= y(t) - \sum_{i=1}^k \hat{\boldsymbol{\psi}}_i^T(t)\hat{\boldsymbol{\alpha}}_i(t-1) \\
\hat{\boldsymbol{\alpha}}_i(t) &= \hat{\boldsymbol{\alpha}}_i(t-1) + \mu(\boldsymbol{\Phi}^{-1} \otimes \mathbf{I}_2)\hat{\boldsymbol{\psi}}_i(t)\varepsilon(t) \\
g_i(t) &= \frac{\hat{\boldsymbol{\chi}}_i^T(t)\hat{\boldsymbol{\alpha}}_i(t-1)\varepsilon(t)}{\hat{\boldsymbol{\alpha}}_i^T(t)(\boldsymbol{\Phi} \otimes \mathbf{I}_2)\hat{\boldsymbol{\alpha}}_i(t)} \\
\hat{\omega}_i(t+1) &= \hat{\omega}_i(t) + \gamma g_i(t) \\
\hat{\boldsymbol{\theta}}_i(t) &= (\mathbf{I}_n \otimes \hat{\mathbf{f}}_i^T(t))\hat{\boldsymbol{\alpha}}_i(t) \\
i &= 1, \dots, k \\
\hat{\boldsymbol{\theta}}(t) &= \sum_{i=1}^k \hat{\boldsymbol{\theta}}_i(t) \\
\hat{s}(t) &= \boldsymbol{\varphi}^T(t)\hat{\boldsymbol{\theta}}(t).
\end{aligned} \tag{18}$$

Frequency-Guided Filter (for $t > t_\omega$):

$$\begin{aligned}
l &= t - t_\omega \\
\bar{\mathbf{f}}_i(l) &= \hat{\mathbf{G}}_i(t)\bar{\mathbf{f}}_i(l-1) \\
\bar{\boldsymbol{\psi}}_i(l) &= \boldsymbol{\varphi}(l) \otimes \bar{\mathbf{f}}_i(l) \\
i &= 1, \dots, k \\
\tilde{\varepsilon}(l) &= y(l) - \sum_{i=1}^k \bar{\boldsymbol{\psi}}_i^T(l)\tilde{\boldsymbol{\alpha}}_i(l-1) \\
\tilde{\boldsymbol{\alpha}}_i(l) &= \tilde{\boldsymbol{\alpha}}_i(l-1) + \mu(\boldsymbol{\Phi}^{-1} \otimes \mathbf{I}_2)\bar{\boldsymbol{\psi}}_i(l)\tilde{\varepsilon}(l) \\
\tilde{\boldsymbol{\theta}}_i(l) &= (\mathbf{I}_n \otimes \bar{\mathbf{f}}_i^T(l))\tilde{\boldsymbol{\alpha}}_i(l) \\
i &= 1, \dots, k \\
\tilde{\boldsymbol{\theta}}(l) &= \sum_{i=1}^k \tilde{\boldsymbol{\theta}}_i(l) \\
\tilde{s}(l) &= \boldsymbol{\varphi}^T(l)\tilde{\boldsymbol{\theta}}(l).
\end{aligned} \tag{19}$$

Output Filter (for $t > t_o$):

$$\begin{aligned}
m &= t - t_o \\
\bar{\boldsymbol{\theta}}_i(m) &= (\mathbf{I}_n \otimes \hat{\mathbf{f}}_i^T(m+t_\omega))\tilde{\boldsymbol{\alpha}}_i(m+t_\alpha) \\
i &= 1, \dots, k
\end{aligned}$$

$$\begin{aligned}
\bar{\boldsymbol{\theta}}(m) &= \sum_{i=1}^k \bar{\boldsymbol{\theta}}_i(m) \\
\bar{s}(m) &= \boldsymbol{\varphi}^T(m)\bar{\boldsymbol{\theta}}(m).
\end{aligned} \tag{20}$$

The quantities $\hat{\boldsymbol{\theta}}_i(t)$, $\tilde{\boldsymbol{\theta}}_i(t)$ and $\bar{\boldsymbol{\theta}}_i(t)$, which appear in (18)–(20), denote estimates of coefficients associated with a particular frequency ω_i (please note that $\boldsymbol{\theta}_i(t)$ is *not* the i th component of $\boldsymbol{\theta}(t)$ —the latter quantity is in this paper denoted by $\theta_i(t)$). The matrices $\hat{\mathbf{G}}_i(t)$ are defined analogously as $\hat{\mathbf{G}}(t)$.

The distributed estimation scheme described above is a parallel structure made up of k identical (from the functional viewpoint) blocks. Each block tracks a particular frequency component $\boldsymbol{\theta}_i(t)$ of the parameter vector $\boldsymbol{\theta}(t) = \sum_{i=1}^k \boldsymbol{\theta}_i(t)$. All subalgorithms are driven by the same “global” prediction error $\varepsilon(t)$. There is an efficient initialization procedure, based on analysis of the so-called system periodogram—evaluated for a short startup fragment of the input/output data—which can be used to identify the number of frequency modes k and to determine initial conditions (both amplitudes and frequencies) needed to start the algorithm practically without initialization transients [20]. Even though this procedure was originally designed for a complex-valued GANF algorithm, its extension to the real-valued case is straightforward.

The signal-oriented ANS version of the three-step GANS algorithm can be derived from (18)–(20) in a similar way as the ANF filter (4) was derived from the GANF algorithm (3).

Finally we note that, as argued in [19], setting $\gamma = n\mu^2$ may be a good way of reducing the number of design degrees of freedom of GANS/ANS algorithms from two (μ, γ) to one (μ) .

VI. SIMULATION RESULTS

Figs. 4, 5, and 6 summarize results of a first simulation experiment arranged to check properties of the proposed system identification algorithm. The simulated system, inspired by channel estimation applications, was governed by

$$y(t) = \theta(t)u(t) + v(t)$$

where

$$\begin{aligned}
\theta(t) &= b(t) \sin(\phi(t) + \phi^o) \\
&= a_1(t) \sin \phi(t) + a_2(t) \cos \phi(t) \\
\phi(t) &= \sum_{s=1}^t \omega(s), \quad \phi^o = \pi/4 \\
a_1(t) &= b(t) \cos \phi^o, \quad a_2(t) = b(t) \sin \phi^o
\end{aligned}$$

i.e., it was a single-tap FIR system ($n = 1$) with a single mode of parameter variation ($k = 1$). The white pseudorandom binary sequence (PRBS) was used as the input signal ($u(t) = \pm 1, \sigma_u^2 = 1$) and the noise was Gaussian with standard deviation $\sigma_v = 0.7$ (average SNR = 0.5 dB) or $\sigma_v = 0.1$ (average SNR = 17 dB).

Fig. 4 shows evolution of the instantaneous amplitude $b(t)$ and the instantaneous frequency $\omega(t)$, along with trajectories of the corresponding estimates obtained from the GANF algorithm

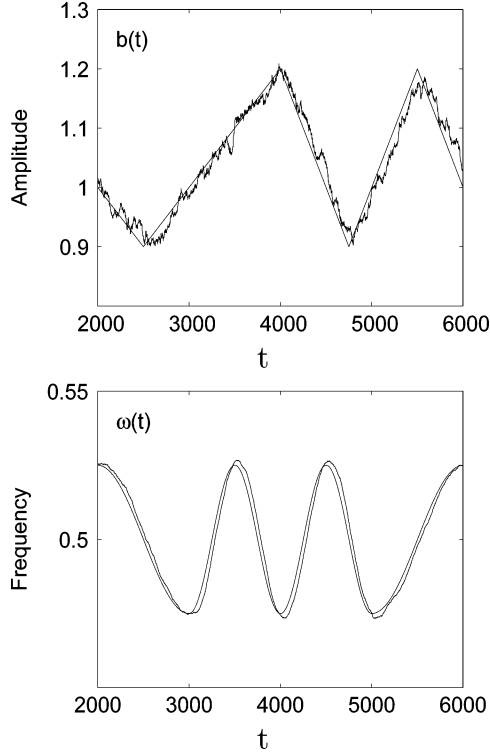


Fig. 4. True system amplitude (upper plot) and frequency (lower plot) changes (smooth lines) and typical trajectories of their estimates (rugged lines) yielded by the GANF algorithm ($\mu = 0.03$, $\gamma = 0.0009$, $\sigma_v^2 = 0.1$).

(2) for $\mu = 0.03$, $\gamma = 0.0009$ and $\sigma_v = 0.1$. Note a clearly visible delay between the true trajectories and the estimated trajectories. Fig. 5 shows how the average accumulated amplitude and frequency matching errors $\Delta_b = \sum_{t=2001}^{6000} (b(t) - \tilde{b}(t + \Delta t))^2$, $\tilde{b}(t) = \sqrt{\tilde{a}_1^2(t) + \tilde{a}_2^2(t)}$ and $\Delta_\omega = \sum_{t=2001}^{6000} (\omega(t) - \hat{\omega}(t + \Delta t))^2$ depend on the choice of the delay Δt . All ensemble averages correspond to 100 different realizations of measurement noise. For the adopted values of μ and γ the nominal delay times are equal to $t_\alpha = \text{int}[2\lambda/\mu] = 65$ and $t_\omega = \text{int}[\mu/\gamma] = 33$ sampling intervals. Note that, in agreement with theory, the nominal time delays are pretty good estimates of the optimal delays (equal to 64 and 37 sampling intervals, respectively)—the corresponding values of $\Delta_b|_{\Delta t=t_\alpha}$ and $\Delta_\omega|_{\Delta t=t_\omega}$ only slightly differ (by 1% and 3%, respectively) from their minimal values.

Fig. 6 presents comparison of the estimation performance of the GANF algorithm and of its two modified versions: the two-step and three-step GANS algorithms. Estimation accuracy of the compared algorithms was measured in terms of the average accumulated output matching errors $\hat{\Sigma}_s = \sum_{t=2001}^{6000} (s(t) - \hat{s}(t))^2$, $\tilde{\Sigma}_s = \sum_{t=2001}^{6000} (s(t) - \tilde{s}(t))^2$ and $\bar{\Sigma}_s = \sum_{t=2001}^{6000} (s(t) - \bar{s}(t))^2$, after the filters have reached their steady state behavior. The plots show how the ensemble averages (100 realizations) of the error statistics depend on the choice of μ (γ was set to μ^2). As expected, delay compensation led to improved tracking results, both in terms of the minimum achievable errors and, more importantly, in terms of the algorithm's robustness to the choice of μ .

The aim of the second simulation experiment was to check estimation properties of the adaptive notch smoother (ANS)- the signal-oriented version of the proposed GANS algorithm. The

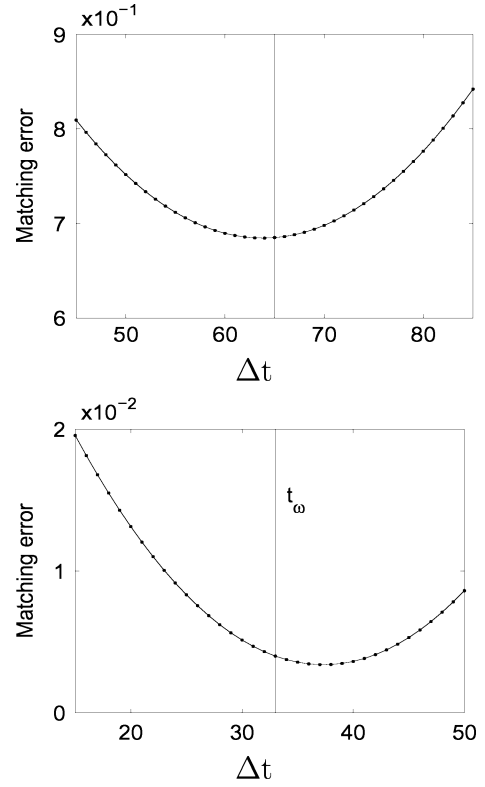


Fig. 5. Dependence of the averaged sums of the squared amplitude matching errors Δ_b (upper plot) and frequency matching errors Δ_ω (lower plot) on the delay Δt ; the nominal delays are marked with vertical lines.

analyzed signal was a mixture of two nonstationary sinusoids embedded in white Gaussian noise

$$\begin{aligned} s(t) &= b_1(t) \sin(\phi_1(t) + \phi_1^o) + b_2(t) \sin(\phi_2(t) + \phi_2^o) \\ &= a_1(t) \sin \phi_1(t) + a_2(t) \cos \phi_1(t) \\ &\quad + a_3(t) \sin \phi_2(t) + a_4(t) \cos \phi_2(t) \\ \phi_1^o &= \pi/4, \quad \phi_2^o = 3\pi/4 \\ \phi_1(t) &= \sum_{s=1}^t \omega_1(s), \quad \phi_2(t) = \sum_{s=1}^t \omega_2(s) \\ y(t) &= s(t) + v(t). \end{aligned}$$

The amplitudes $b_1(t), b_2(t)$ and the instantaneous frequencies $\omega_1(t), \omega_2(t)$ were governed by random walk models, driven by mutually independent white noise sequences with standard deviations $\sigma_{\Delta b_1} = \sigma_{\Delta b_2} = 0.001$ and $\sigma_{\Delta \omega_1} = \sigma_{\Delta \omega_2} = 0.001$, respectively.

Fig. 7 shows dependence of the average accumulated signal matching errors $\hat{\Sigma}_s, \tilde{\Sigma}_s$ and $\bar{\Sigma}_s$ (defined analogously as in the system case) on the adaptation gain μ for two values of the average SNR (0 and 12 dB), corresponding to $\sigma_v = 2$ and $\sigma_v = 0.5$, respectively. The second adaptation gain γ was set to μ^2 . It is worth noticing that when, instead of ANF, the classical linear prediction adaptive filters (exponentially weighted least squares or least mean squares) are used to enhance quasi-periodically varying signals buried in noise, the corresponding signal matching errors increase at least several times; therefore, from the practical viewpoint, the advantage of using adaptive notch filtering is obvious. Finally, Fig. 8 shows dependence of the signal matching errors on SNR for a fixed value of μ ($\mu =$

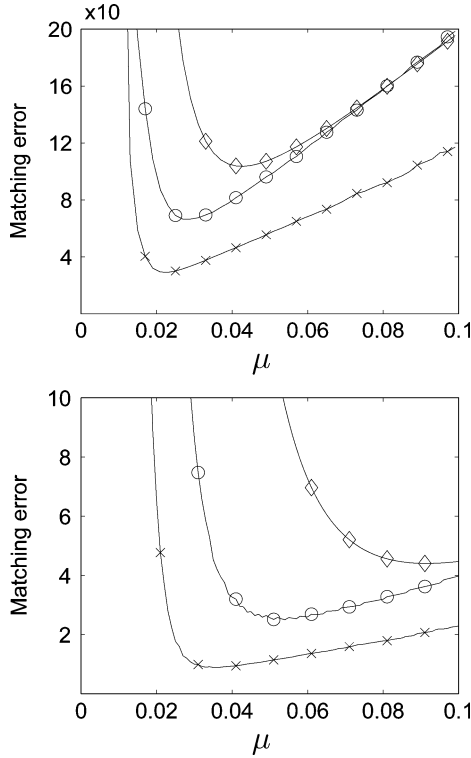


Fig. 6. Dependence of the averaged sums of the squared output matching errors $\hat{\Sigma}_s$, $\hat{\Sigma}_s$ and $\hat{\Sigma}_s$ on the adaptation gain μ for two average SNR rates: SNR = 0.5 dB (upper figure) and SNR = 17 dB (lower figure). Comparison involves the estimates yielded by the original GANF algorithm (\diamond), the two-step GANS algorithm (\circ) and a three-step GANS algorithm (\times). All plots were evaluated on a grid of 100 equidistant values of μ .

0.05). Similarly as in the system case, the advantages of using the proposed three-step smoothing procedure are evident.

VII. CONCLUSION

GANFs are devices used to estimate coefficients of quasi-periodically varying systems. It was shown that compensation of estimation delays, arising in the amplitude tracking and frequency tracking loops of GANF algorithms, can be regarded a computationally efficient form of smoothing. The proposed solution is a cascade of three filters. The “pilot” filter provides preliminary (biased) amplitude and frequency estimates. The debiased (delayed) frequency estimates yielded by the pilot algorithm are fed into the second algorithm—the “frequency-guided” generalized adaptive notch filter. Finally, the third, “output” filter, is used to combine the debiased (delayed) amplitude estimates, provided by the frequency-guided algorithm, with the debiased frequency estimates obtained earlier. The three-step GANS provides better results, both in terms of estimation accuracy and in terms of robustness to the choice of design parameters, than the original GANF algorithm and the recently proposed two-step GANS procedure.

APPENDIX

Tracking properties of the unnormalized GANF algorithm were studied in [1]. The only difference between the unnormal-

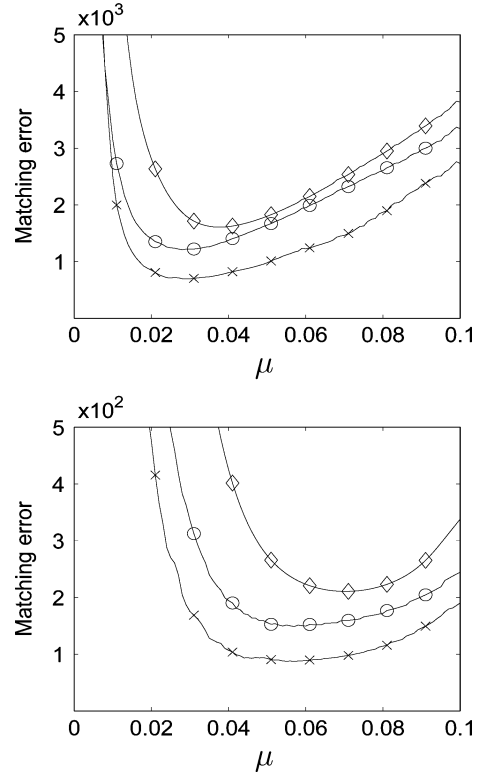


Fig. 7. Dependence of the averaged sums of the squared signal reconstruction errors $\hat{\Sigma}_s$, $\hat{\Sigma}_s$ and $\hat{\Sigma}_s$ on the adaptation gain μ for two average SNR rates: SNR = 0 dB (upper figure) and SNR = 12 dB (lower figure). Comparison involves the estimates yielded by the original GANF algorithm (\diamond), the two-step GANS algorithm (\circ), and a three-step GANS algorithm (\times). All plots were evaluated on a grid of 100 equidistant values of μ .

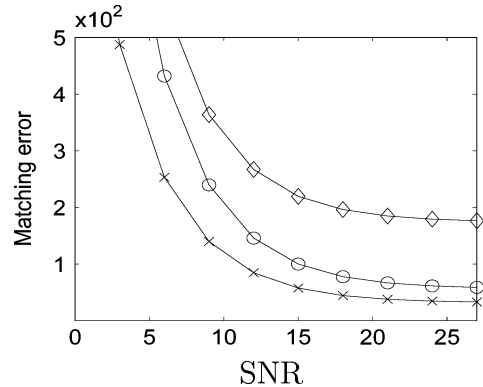


Fig. 8. Dependence of the averaged sums of the squared signal reconstruction errors $\hat{\Sigma}_s$, $\hat{\Sigma}_s$ and $\hat{\Sigma}_s$ on the average SNR rate for a fixed value of μ ($\mu = 0.05$). Comparison involves the estimates yielded by the original GANF algorithm (\diamond), the two-step GANS algorithm (\circ), and a three-step GANS algorithm (\times). All plots were evaluated on a grid of 10 equidistant values of SNR.

ized algorithm and the normalized one lies in some details of the frequency tracking loop, which in the first case has the form

$$g(t) = \hat{\chi}^T(t) \hat{\alpha}(t-1) \varepsilon(t)$$

$$\hat{\omega}(t+1) = \hat{\omega}(t) + \eta g(t).$$

For the unnormalized algorithm one obtains (see (12) in [1])

$$\Delta \hat{\omega}(t) \cong H_1(q^{-1})e(t) + H_2(q^{-1})w(t) \quad (21)$$

where

$$\begin{aligned}\Delta\hat{\omega}(t) &= \hat{\omega}(t) - \omega(t), \\ e(t) &= \boldsymbol{\alpha}_o^T \boldsymbol{\chi}(t)v(t), w(t) = \omega(t) - \omega(t-1), \\ H_1(q^{-1}) &= \frac{2(1-\delta)(1-q^{-1})q^{-1}}{b^2(1-(\lambda+\delta)q^{-1} + \lambda q^{-2})} \\ H_2(q^{-1}) &= -\frac{1-\lambda q^{-1}}{1-(\lambda+\delta)q^{-1} + \lambda q^{-2}}\end{aligned}$$

and

$$\lambda = 1 - \mu/2, \quad \delta = 1 - \eta b^2/2$$

Note that (21) can be rewritten in the form

$$\hat{\omega}(t) \cong H_1(q^{-1})e(t) + [1 + (1 - q^{-1})H_2(q^{-1})]\omega(t). \quad (22)$$

When scaling is introduced, i.e.,

$$\begin{aligned}g(t) &= \frac{\hat{\boldsymbol{\chi}}^T(t)\hat{\boldsymbol{\alpha}}(t-1)\varepsilon(t)}{\hat{\boldsymbol{\alpha}}^T(t)(\boldsymbol{\Phi} \otimes \mathbf{I}_2)\hat{\boldsymbol{\alpha}}(t)} \cong \frac{\hat{\boldsymbol{\chi}}^T(t)\hat{\boldsymbol{\alpha}}(t-1)\varepsilon(t)}{b^2} \\ \hat{\omega}(t+1) &= \hat{\omega}(t) + \gamma g(t)\end{aligned}$$

the relationship (21) does not change except that η should be replaced with γ/b^2 , leading to $\delta = 1 - \gamma/2$. One can easily check that in this case (22) is identical with (5).

REFERENCES

- [1] M. Niedźwiecki and A. Sobociński, "On tracking properties of real-valued generalized adaptive notch filters," *IEEE Trans. Signal Process.*, vol. 55, no. 5, pt. 1, pp. 1688–1695, 2007.
- [2] M. K. Tsatsanis and G. B. Giannakis, "Modeling and equalization of rapidly fading channels," *Int. J. Adapt. Control Signal Process.*, vol. 10, pp. 159–176, 1996.
- [3] G. B. Giannakis and C. Tepedelenlioğlu, "Basis expansion models and diversity techniques for blind identification and equalization of time-varying channels," *Proc. IEEE*, vol. 86, pp. 1969–1986, 1998.
- [4] J. Bakkoury, D. Roviras, M. Ghogho, and F. Castanie, "Adaptive MLSE receiver over rapidly fading channels," *Signal Process.*, vol. 80, pp. 1347–1360, 2000.
- [5] J. K. Tugnait and W. Luo, "Linear prediction error method for blind identification of periodically-varying channels," *IEEE Trans. Signal Process.*, vol. 50, pp. 3070–3082, 2002.
- [6] M. Niedźwiecki and P. Kaczmarek, "Tracking analysis of a generalized adaptive notch filter," *IEEE Trans. Signal Process.*, vol. 54, pp. 304–314, 2006.
- [7] B. Widrow and S. D. Stearns, *Adaptive Signal Processing*. Englewood Cliffs, NJ: Prentice-Hall, 1985.
- [8] M. Soderstrand, T. G. Johnson, R. H. Strandberg, H. H. Loomis Jr., and K. V. Rangarao, "Suppression of multiple narrow-band interferences using real-time adaptive notch filters," *IEEE Trans. Circuits Syst.—II*, vol. 44, pp. 217–225, 1997.
- [9] C. R. Fuller and A. H. von Flotow, "Active control of sound and vibration," *IEEE Syst. Contr. Mag.*, vol. 15, pp. 9–19, 1995.

- [10] Y. Chen, V. Wickramasinghe, and D. Zimcik, "Smart spring impedance control algorithm for helicopter blade harmonic vibration suppression," *J. Vib. Contr.*, vol. 11, pp. 543–560, 2005.
- [11] N. V. Thakor and Y. S. Zhou, "Application of adaptive filtering to ECG analysis: Noise cancellation and arrhythmia detection," *IEEE Trans. Biomed. Eng.*, vol. 38, pp. 785–794, 1991.
- [12] M. Ferdjallah and R. E. Barr, "Adaptive digital notch filter design on the unit circle for the removal of powerline noise from biomedical signals," *IEEE Trans. Biomed. Eng.*, vol. 41, pp. 529–536, 1994.
- [13] W. K. Ma, Y. T. Zhang, and F. S. Yang, "A fast recursive-least-squares adaptive notch filter and its applications to biomedical signals," *Med. Biol. Eng. Comput.*, vol. 37, pp. 99–103, 1999.
- [14] M. Niedźwiecki and A. Sobociński, "A simple way of increasing estimation accuracy of generalized adaptive notch filters," *IEEE Signal Process. Lett.*, vol. 14, pp. 217–220, 2006.
- [15] P. Hedelin, "Can the zero-lag filter be a good smoother?," *IEEE Trans. Inf. Theory*, vol. IT-23, pp. 490–499, 1977.
- [16] P. Hedelin and I. Jönsson, "Applying a smoothing criterion to the Kalman filter," *IEEE Trans. Autom. Control*, vol. AC-23, pp. 916–921, 1978.
- [17] M. Niedźwiecki, *Identification of Time-Varying Processes*. New York: Wiley, 2000.
- [18] T. Söderström, T. Stoica, and P. Stoica, *System Identification*. Englewood Cliffs, NJ: Prentice-Hall, 1988.
- [19] M. Niedźwiecki and P. Kaczmarek, "Generalized adaptive notch filter with a self-optimization capability," *IEEE Trans. Signal Process.*, vol. 54, pp. 4185–4193, 2006.
- [20] M. Niedźwiecki and P. Kaczmarek, "Identification of quasi-periodically varying systems using the combined nonparametric/parametric approach," *IEEE Trans. Signal Process.*, vol. 53, pp. 4588–4598, 2005.



Maciej Niedźwiecki was born in Poznań, Poland, in 1953. He received the M.Sc. and Ph.D. degrees from the Gdańsk University of Technology, Gdańsk, Poland, and the Dr.Hab. (D.Sc.) degree from the Technical University of Warsaw, Warsaw, Poland, in 1977, 1981, and 1991, respectively.

He spent three years as a Research Fellow with the Department of Systems Engineering, Australian National University (1986–1989). He is currently a Professor and Head of the Department of Automatic Control, Faculty of Electronics, Telecommunications and Computer Science, Gdańsk University of Technology. His main areas of research interests include system identification, signal processing, and adaptive systems. He is the author of the book *Identification of Time-varying Processes* (New York: Wiley, 2000).

Dr. Niedźwiecki served as a Vice Chairman of the Technical Committee on Theory of the International Federation of Automatic Control (IFAC) during 1990–1993.



Adam Sobociński received the M.Sc. degree in telecommunication from Gdańsk University of Technology, Gdańsk, Poland, in 1996.

Since 1996, he has been working as an Assistant Professor in the Department of Information Systems, Faculty of Electronics, Telecommunications and Computer Science, Gdańsk University of Technology, where he is currently pursuing the Ph.D. degree. His interests include system identification and adaptive filtering, as well as digital signal processing of audio and telecommunication signals.